Chemical and Process Engineering 2014, 35 (3), 369-385
DOI: 10.2478/cpe-2014-0028

NUMERICAL ANALYSIS OF MIXING UNDER LOW AND HIGH FREQUENCY PULSATIONS AT SERPENTINE MICROMIXERS

Ziemowit M. Malecha*[1,2], Karol Malecha[3]

[1] University of New Hampshire, Program in Integrated Applied Mathematics, Durham, NH 03824, USA

[2] Wrocław University of Technology, Department of Cryogenic, Aviation and Process Engineering, Wybrzeże Wyspiańskiego 27, 50-370 Wrocław, Poland

[3]Wrocław University of Technology, Faculty of Microsystem Electronics and Photonics, Wybrzeże Wyspiańskiego 27, 50-370 Wrocław, Poland

The numerical investigation of the mixing process in complex geometry micromixers, as a function of various inlet conditions and various micromixer vibrations, was performed. The examined devices were two-dimensional (2D) and three-dimensional (3D) types of serpentine micromixers with two inlets. Entering fluids were perturbed with a wide range of the frequency (0 – 50 Hz) of pulsations. Additionally, mixing fluids also entered in the same or opposite phase of pulsations. The performed numerical calculations were 3D to capture the proximity of all the walls, which has a substantial influence on microchannel flow. The geometry of the 3D type serpentine micromixer corresponded to the physically existing device, characterised by excellent mixing properties but also a challenging production process (Malecha et al., 2009). It was shown that low-frequency perturbations could improve the average mixing efficiency of the 2D micromixer by only about 2% and additionally led to a disadvantageously non-uniform mixture quality in time. It was also shown that high-frequency mixing could level these fluctuations and more significantly improve the mixing quality. In the second part of the paper a faster and simplified method of evaluation of mixing quality was introduced. This method was based on calculating the length of the contact interface between mixing fluids. It was used to evaluate the 2D type serpentine micromixer performance under various types of vibrations and under a wide range of vibration frequencies.

Keywords: Serpentine micromixer, active mixing, numerical simulations, LTCC technology

1. INTRODUCTION

Modern analytical procedures used in chemical, biological or biochemical studies, consists of several steps: sampling, carrying out scheduled (bio)chemical reactions under appropriate conditions, separation and assaying products. Classical methods of instrumental analysis are characterised by the extended period of detection of the product, large consumption of reagents and significant amounts of waste. The way to cope with these difficulties is with the introduction of miniaturised analytical systems such as μTAS (Micro-Total Analysis System) or Lab-on-chip. These microsystems make it possible to perform various (bio)chemical reactions and analyses in a continuous and fully automated mode, on samples in which the volumes are of micro or nanoliters. This can significantly reduce the amount of needed chemicals and also shorten the amount of time needed to assay the considered

*Corresponding author, e-mail: ziemowit.malecha@pwr.edu.pl

substances. The beginning of the development of this type of equipment dates back to the early 1990s (Gravesen et al., 1993; Manz et al., 1990).

Some of the first examples of realizations and testing of microchips were e.g.: integrated miniature gas chromatograph (Dziuban et al., 2004), thermocycler for DNA replication (Liu et al., 2011) and microsystem for dialysis based on the determination of glucose, lactate, glutamate and potassium ions (Malecha et al., 2011). Modern microfluidic systems typically consist of several integrated modules which are responsible for the following steps: transportation of the sample (micropumps , microvalves), initial preparation of the sample (mixer), reaction (microreactor) and detection. One of the key elements of such devices is a micromixer able to efficiently mix a very small quantity of liquid.

Mixing is a process during which the concentration of ingredients in the system is equalised. Fluid elements of different ingredients move with respect to each other, which leads to turbulent or molecular diffusion processes (Ottino and Wiggins, 2004). An appropriate rate of mixing is essential for the desired functioning of microchips. A good example can be the chemical reaction involving the catalyst (e.g. enzyme), which requires all reactants to be well mixed before they reach the reactor with catalytic bed. When mixing is too slow with respect to the rate of chemical reaction, the performance of the ongoing process can be significantly impaired, which can result in a final product of undesirable composition and properties.

Microfluidic systems, because of their small dimensions, are dominated by laminar flows, which significantly impairs mixing efficiency. The mass transfer between the mixed fluids can take place only by either molecular diffusion or deformation of fluid elements (chaotic advection) (Gravesen et al., 1993; Wiggins and Ottino, 2004). The rate of molecular diffusion is characterised by molecular diffusion coefficient D. Its value depends mainly on the type of fluid (size of the molecule) and its temperature. D increases with decreasing size of the molecules and increasing temperature. Unfortunately, most organic molecules used in (bio)chemical analysis have a relatively large size ($\sim 10^{-9}$ m). In addition organic substances are very sensitive to elevated temperature. High temperature can lead to annealing or decomposition of the organics. In consequence, organic chemicals used in (bio)chemical analysis are characterised with a very small diffusion coefficients D ($\sim 10^{-9}$ m^{2}s^{-1}).

On the other hand, mixing can be enhanced by increasing the contact area between reagents by the appropriate deformation of fluid elements. An increase in contact area is dependent on the type of flow, the gradients of fluid velocity which determines the rate of deformation, and the initial orientation of the contact surface of mixed fluids. Moreover, if the mixing fluids differ in viscosity, this, too, will affect the micromixing process. The size of the contact area also has an influence on the rate of diffusion of the mixing fluids. It maintains higher concentration gradients longer between mixture components and makes molecular diffusion faster according to Fick's first law,

$$\frac{1}{s}\frac{dm}{dt} = -D\nabla c \tag{1}$$

where S – is a size of the contact (interface) area between fluids (m^2) and m is the amount of substance that flows through the interface area during time t. The term $\frac{1}{s}\frac{dm}{dt}$ is also called the diffusion flux and it is designated as J.

A larger interface area results in a larger area for mass transfer, and higher concentration gradients accelerate the diffusion process. The rate of fluid element deformation is mainly impacted by the flow field, the shape of the fluid elements, and the difference in viscosity of the mixed fluids (Bałdyga and Bourne, 1984). The deformation of fluid elements is achieved by the suitable design of the micromixer. There are two main types of micromixers: active and passive (Hessel et al., 2005; Nguyen and Wu, 2005). In the active mixers, deformation of the fluid elements is achieved by perturbation of the flow by external effects (pressure, temperature, electric field , magnetic field, acoustic waves, etc.), whereas,

in the case of passive mixers, fluid elements are deformed as a result of the flow through the channel of a complex geometry.

The results presented in the works presented by Groß et al. (2008), Malecha et al., (2009) and Yi and Bau (2003) showed that the properly designed geometry of the micromixer could lead to significant improvement in mixing efficiency of two fluids. However, the micromixers had a rather complex geometry, and their production, using known microengineering techniques, could be very challenging and time consuming. In the work (Malecha et al., 2009) it was shown that the 3D type serpentine mixer had very high mixing efficiency but would be very challenging to manufacture. Figure 1 shows the micromixer and its manufacturing process, made with LTCC (Low Temperature Co-fired Ceramics) technology, which was studied in that work.

It consists of three LTCC layers. The bottom layer defines the base of the micromixer. The 3D serpentine channel is fabricated in the middle and top layers. The micromixer is sealed with a transparent cover plate made of PDMS (polydimethylosiloxane). The polymer was bonded to the LTCC structure using plasma oxidation process. Details on the PDMS-LTCC microfluidic system fabrication process can be found in (Malecha, 2013).

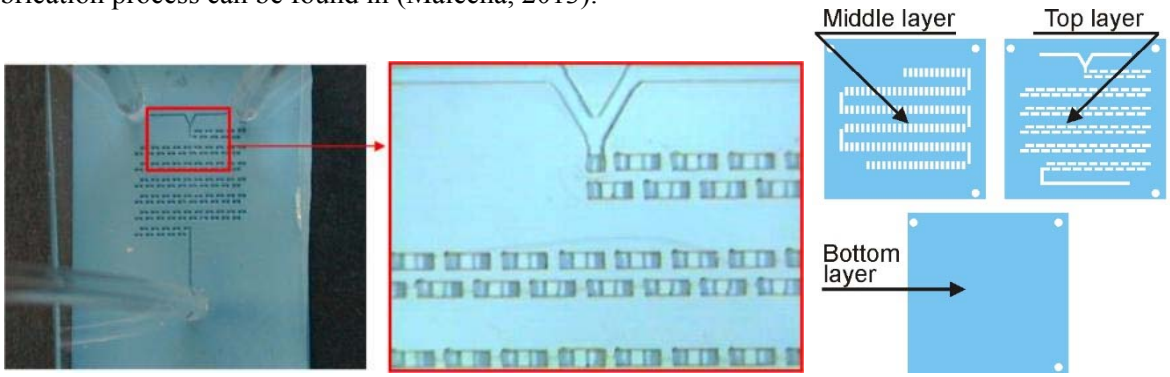

Fig. 1. Left: 3D type serpentine micromixer made with LTCC technology. Right: LTCC layers for fabrication of the micromixer

Despite its high efficiency, it is possible that an undesired phenomenon could manifest itself during its performance. Complex geometry of the micromixer may lead to generation of air microbubbles inside its microchannels. Bubble generation is a quite well known phenomenon in microfluidics. It results in breaking the continuity of the liquid phase. Break-up of the fluid continuity can be caused by a shear stress or pressure drop. The pressure drop comes from the high hydraulic resistance to flow of the liquid across the microchannel. Hydraulic resistance strongly depends on channel geometry. It increases with increasing number of bends, therefore 3D serpentine micormixer is characterised with a relatively high hydraulic resistance (Nguyen, 2012). In microfluidic systems with an integrated optical or electrochemical detection unit, the presence of air microbubbles in liquid phase can generate additional noise to the output signal and can also attenuate this signal. One way to avoid both technological and performance difficulties, is to choose the simpler, 2D type serpentine mixer. Unfortunately, lower mixing efficiency can be expected.

A solution to this problem was presented by Oberti et al. (2009), and Nelid et al. (2010). In the work by Oberti et al. (2009), the authors showed that mixing can be improved under the low frequency vibration of the whole microchip, whereas, Neild et al. (2010), demonstrated a possibility in mixing improvement from low frequency pulsations of the entering fluid. Similar conclusions can be found in the paper by Glasgow et al. (2003) where the numerical analysis showed that mixing in the 2D T-shaped microchip was improved by low frequency (5 Hz) pulsations at one of the inlets. The above mentioned studies were limited to low frequency perturbations and simple geometry channels. The authors did not demonstrate how mixing qualities changed with time or under high frequency perturbations. In our

study, we will explore a wide range of the frequency pulsations applied at both inlets in various configurations. We will also explore the influence of different types of vibrations applied to the whole microchip.

In our work, we have numerically investigated the influence of both low and high frequency perturbations in the three-dimensional calculations of the mixing process, but in complex geometry channels. Two- and three-dimensional serpentine micromixers were examined. We have studied different inlet conditions where fluids were entering in the same or in the opposite phase of pulsations. We have shown that low-frequency perturbations can improve the average mixing efficiency by only little above 2% and lead to a non-uniform mixture quality in time, at the exit from the micromixer. These fluctuations in mixing quality are directly related to the applied pulsations and their amplitude can be significant. It was shown that high-frequency mixing can level these fluctuations and even improve overall mixing.

2. MATHEMATICAL MODEL

In our work, the mixing process of two fluids was modelled by solving the convection-diffusion equation for concentration c:

$$\frac{\partial c}{\partial t} + \mathbf{u} \cdot \nabla c = D \nabla^2 c \tag{2}$$

where $\mathbf{u}=(u, v, w)$ is the fluid velocity and D is the mass diffusion coefficient. Concentration $c = 1$ means pure phase 1 and $c = 0$ means pure phase 2. Any value between 0 and 1 relates to the mixture of a certain concentration c of the first fluid within the second fluid. From Equations (1) and (2), it can be deduced that mixing is more efficient if the interface area between two fluids is larger and also if the concentration gradients between two mixing fluids are higher. It is a well-known property of diffusion (represented by the right side term of Equation (1)) that larger contact area between areas of different concentrations results in higher mass flux. On the other hand, for advection dominated flows (high Reynolds number), mass transfer is significantly intensified by turbulent mixing accompanied with phenomena such as the eruption of the boundary layer. This occurrence can be provoked by the vortex structure in the bulk flow and leads to the abrupt ejection of the fluid from the near wall regions to the interior of the flow (Kudela and Malecha, 2009).

Microchannel flows are strictly laminar and their mixing process is dominated by diffusion only. The only way to improve it, is with an artificial creation of additional complexity of the flow field. This can be obtained by increasing the contributions of the convection part in Equation (1). That can be achieved with a properly designed mixer which will strongly stretch and fold the fluid elements, or by introducing some perturbations at the inlets.

The velocity field was calculated by solving incompressible Navier-Stokes equations (Batchelor, 2000):

$$\frac{\partial(\rho \mathbf{u})}{\partial t} + \nabla \cdot (\rho \mathbf{u}\mathbf{u}) = -\nabla p + \nabla \cdot \mu \nabla \mathbf{u} + F \tag{3}$$

$$\nabla \cdot (\rho \mathbf{u}) = 0 \tag{4}$$

where ρ and μ are the density and dynamics viscosity of the mixture, p is the pressure and F is the force related to gravity arising from density variability of the mixture. The above equations were solved using the *twoMixingFluidsFoam* solver implemented in *OpenFOAM* (Open Source Field Operation and Manipulation) (OpenFOAM, 2009). OpenFOAM is an open-source numerical library for solving partial differential equations (PDEs) in arbitrary 3D geometries, based on the Finite Volume Method

(http://www.openfoam.com/) and one which has been used effectively in a variety of challenging applications (Malecha, 2011).

2.1. Two-Mixing-Fluids Model

From the macroscopic perspective, an incompressible fluid can be characterised by its density and viscosity. Two different fluids can be distinguished through these physical properties. For the first fluid, we can write: ρ_1 and μ_1 and for the second: ρ_2 and μ_2. The density and viscosity of the mixture at any point in the domain are calculated as a weighted average of the concentration of the two fluids:

$$\rho = c\rho_1 + (1-c)\rho_2 \tag{5}$$

and

$$\mu = c\mu_1 + (1-c)\mu_2 \tag{6}$$

Despite the fact that the approximation (6) is not physically valid, it was adopted in OpenFOAM solvers. Physically appropriate approximations can be found in (Monnery et al., 1995). In order to avoid any inconsistencies which could arise from using Equation (6), the same value of viscosity was assumed for both fluids in the present studies.

The two-mixing-fluids model can be adapted to more challenging flows, where density and viscosity are e.g. a function of temperature (Malecha et al., 2013).

3. CALCULATIONS SET-UP

In the first part of the Results section we will consider seven different scenarios of the inlet boundary conditions (BCs):

- Constant velocity on both inlets (Const).
- Low frequency pulsations on one inlet and constant velocity on the second inlet (*L1c*).
- Low frequency pulsations, in the same phase, on both inlets (L_{in}).
- Low frequency pulsations, in the opposite phase, on both inlets (L_{out}).
- High frequency pulsations on one inlet and constant velocity on the second inlet (*H1c*).
- High frequency pulsations, in the same phase, on both inlets (H_{in}).
- High frequency pulsations, in the opposite phase, on both inlets (H_{out}).

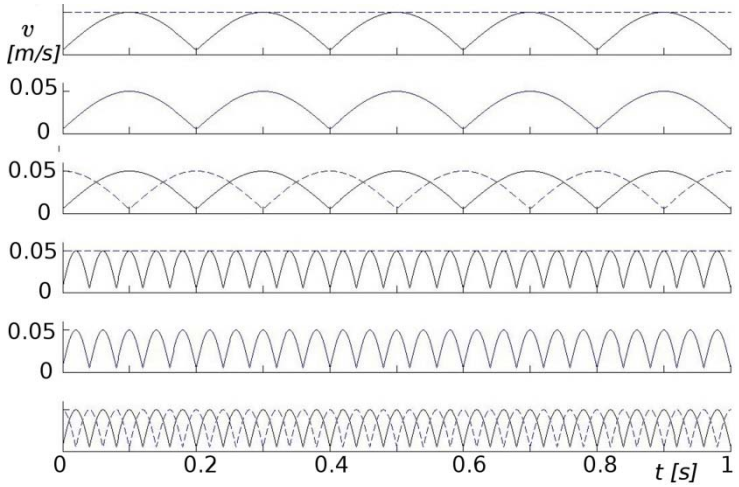

Fig. 2. Different types of BC used in the study. The solid line corresponds to the first inlet, the dashed line to the second one. Low frequency oscillations are 5Hz, high are 25Hz.

The first case will serve as a reference for the others. Abbreviations in the brackets are used later in the descriptions of the figures. Figure 2 summarises graphically the above scenarios. The solid line corresponds to the first inlet, the dashed line to the second one. The mathematical formulations of the used velocity BC are:

$$v = 0.05$$
$$v = 0.05 + \left|0.045\sin(5\pi t)\right| \tag{7}$$
$$v = 0.05 + \left|0.045\cos(5\pi t)\right|$$

where v [ms^{-1}] is the velocity component in the y (vertical) direction and $0 \le t \le 1$ is the time in seconds.

Numerical models of the investigated microchips with exemplary results are depicted in Figs. 3 and 4. Figure 4 shows the numerical model of the 3D type serpentine micromixer presented in Fig. 1. Its simplified version is illustrated in Fig. 3: 2D type serpentine mixer, which bends in two directions only. The size of the 2D microchip is (x, y, z) = (length, height, width) = (48, 33, 1.5)×10^{-4} m. Its mixing section has 12 bends and a total length of 81×10^{-4} m, whereas the size of the 3D microchip is (x, y, z) = (length, height, width) = (33, 33, 1.5)×10^{-4} m. Its mixing section has 20 bends and the total length of 120×10^{-4} m. The two-dimensional cross-section of the channel is the same for both microchips: (y, z) = (height, width) = (3, 1.5)×10^{-4} m. The capital letters **A** and **B** mark the places where detailed measurements were taken. Measurements were taken along the vertical cross-sections in two locations: in the middle of the channel (A_c, B_c) and close to the wall (A_w, B_w). Measurements taken closer to the wall may be, in fact, more informative because flow in the microchannels is very much constrained by the proximity of the walls. This fact is significantly violated in the two-dimensional calculations, because they assume an infinitely wide channel in the third direction (hence no influence of the wall in that direction).

Location **A** is relatively close to the T-junction, whereas **B** is at the end of the mixing section of the channel. The results in location **A** and **B** will show comprehensive information about the influence of the different type of considered BC on the mixing efficiency. An additional conclusion will be deduced by comparative results in locations **A** and **B**.

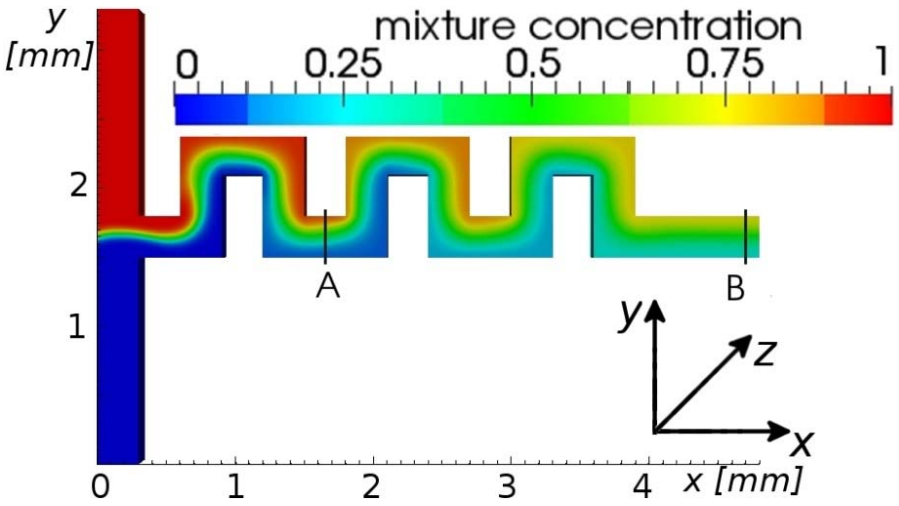

Fig. 3. 3D numerical model of the 2D type serpentine micromixer used in the calculations. The mixing channel bends in two directions. Letters **A** and **B** show where detailed measurements were taken. Figure shows exemplary results for the L_{in} BC and time t = 0.5 s

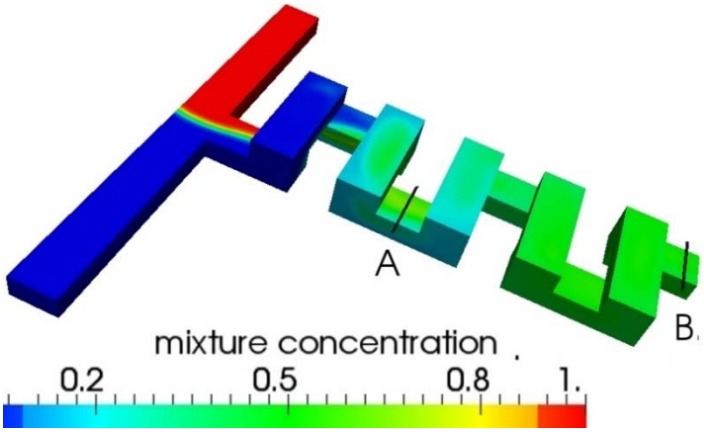

Fig. 4. 3D numerical model of the 3D type serpentine micromixer used in the calculations. The mixing channel bends in three directions. Letters **A** and **B** show where detailed measurements were taken. Figure shows exemplary results for the H_{out} BC and time t = 1 s

To evaluate and compare the degree of mixing for different BCs, we will calculate normalised standard deviation along each cross-section as follows:

$$\sigma = 1 - \frac{\sqrt{\frac{1}{H}\int_0^H (c(y)-\alpha)^2 dy}}{\alpha} \tag{8}$$

where H is the height of the channel in the vertical y direction, $c(y)$ is the change of the concentration along the considered cross-section and α = 0.5 is the mean value corresponding to complete (full) mixing. Here σ = 1 denotes ideal mixing and σ = 0 segregated flow. The above formula can be imprecise in our case, because mass flux is also changing along the cross-section - closer to the walls, flow elements travel slower. That is why, similarly as in (Glasgow, 2003) we will introduce weighted standard deviation (DM) as an improved measure of the degree of mixing:

$$DM = 1 - \frac{\sqrt{\frac{1}{H}\int_0^H (c(y)-\alpha)^2 \frac{u(y)}{u_m} dy}}{\alpha} \tag{9}$$

where $u(y)$ is the horizontal component of the velocity vector along the cross-section and $u_m = \frac{1}{H}\int_0^H u(y)dy$ is the mean horizontal velocity in that cross-section. Similarly, like before, DM = 1 indicates ideal mixing. Both σ and DM are functions of time, and as will be shown later, they can change significantly with time, which might be unacceptable for microchip performance.

Table 1. Fluid properties

Fluid parameter	Value
ρ, density [kgm^{-3}]	10^3
μ, dynamic viscosity [Pa·s]	10^{-3}
D, diffusion coefficient [m^{2}s^{-1}]	10^{-9}

The physical characteristics of the considered fluids are shown in Table 1. These values are representative for aqueous solutions which are often used in microfluidic devices. In our case, Reynolds number $Re = \frac{UHp}{\mu} \sim O(1)$, where U is a characteristic velocity of the flow (in the considered flow it is

equal to the time-averaged velocity BC at the inlet, Equation (7) and H is the characteristic size of the microchannel (height of the channel).

4. RESULTS, PART I

4.1. Quality of mixing in the A location of the 2D type serpentine mixer

The upper row of Fig. 5 shows how standard deviation σ changes in time for low and high frequency pulsations in the cross-section A_C located in the centre of the channel. It can be seen that, relatively close to the T-junction, the influence of the BC pulsations is still very strong, producing a significantly non-uniform quality of mixing in time. In the case of in-phase pulsations, these fluctuations are weaker, whereas in the out-of-phase BC, they are magnified. The constant line corresponds to the reference case with constant BC at both inlets.

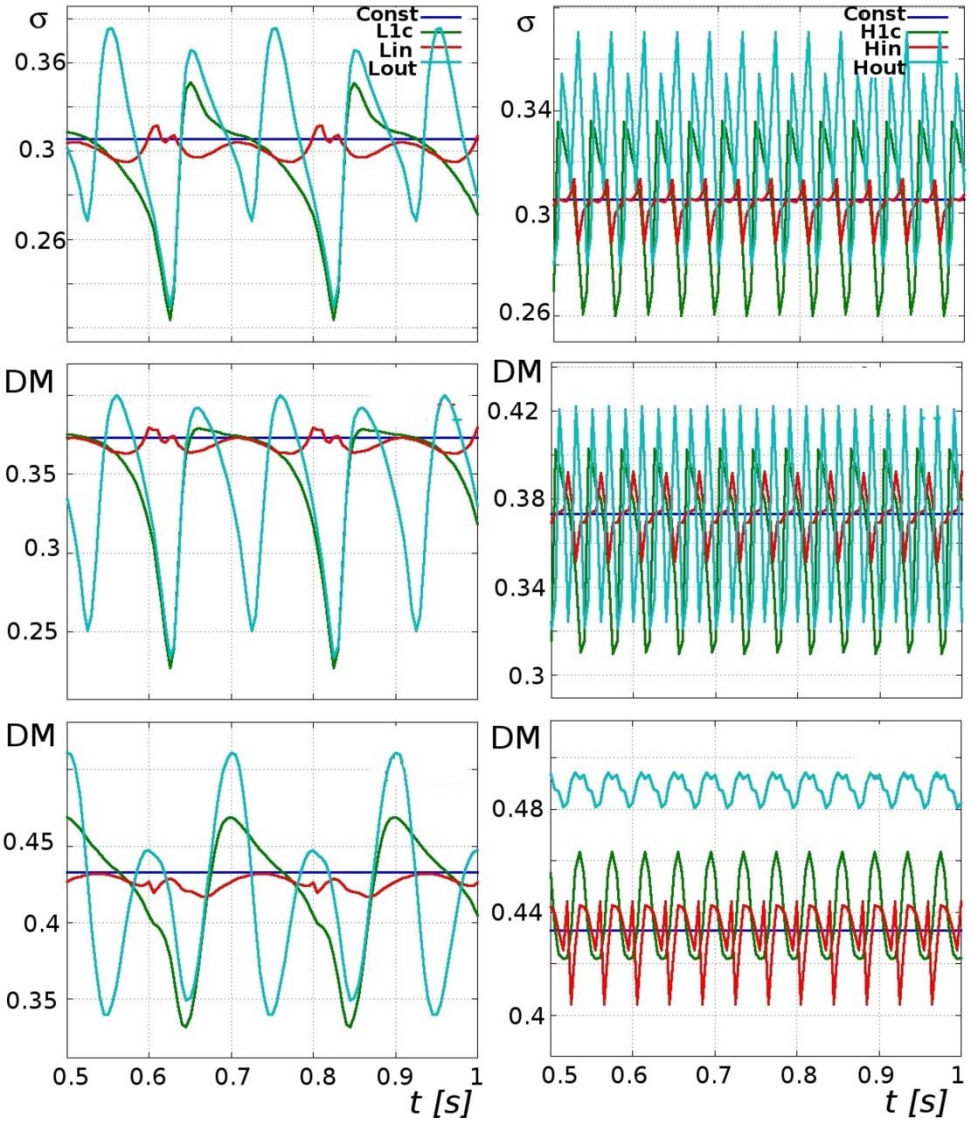

Fig. 5. Changes of σ (upper row) and DM (middle and lower rows) in time in the A_C (upper and middle rows) and A_W (lower row) cross-sections. The left column shows low frequency results and the right column shows high frequency results. The horizontal axis shows time in seconds

Table 2 shows the time averaged values of σ (second column). Every row corresponds to the different type of BC and is listed in the same order as enumerated flow scenarios from the beginning of this section. Compared to the reference case from the first row, it can be seen that pulsations cannot improve mixing at this location.

Table 2. σ and *DM* averaged in time in the A_C and A_W cross-sections

BC type	σ at A_C	σ at A_W	*DM* at A_C	*DM* at A_W
1 – Const	0.305	0.359	0.373	0.433
2 – *L1c*	0.294	0.358	0.350	0.422
3 – L_{in}	0.301	0.354	0.369	0.426
4 – L_{out}	0.305	0.378	0.338	0.418
5 – *H1c*	0.304	0.370	0.363	0.438
6 – H_{in}	0.303	0.358	0.373	0.432
7 – H_{out}	0.326	0.420	0.368	0.488

The middle row of Figure 5 and the third column of Table 2 compare the quality of the mixing, calculated using the DM parameter, Equation (9). Here, the conclusions are similar to those of parameter σ. The consecutive results will be limited to DM only. As previously mentioned, this parameter is more precise for this type of analysis because mass flux is changing along the considered cross-sections.

Analysing data from the cross-section close to the wall (location A_w), the lower row of the Figure 5 and the fourth column of Table 2, we can see that BC with high frequency and out-of-phase pulsations leads to slightly better mixing than that in the reference case. Out-of-phase pulsations prevail over in-phase pulsation BC in one more important aspect. The amplitude of oscillations at A_w is suppressed, which means that the quality of the mixture is less influenced by BC. However, the general conclusion is that applying various types of BC cannot significantly improve mixing at location **A**.

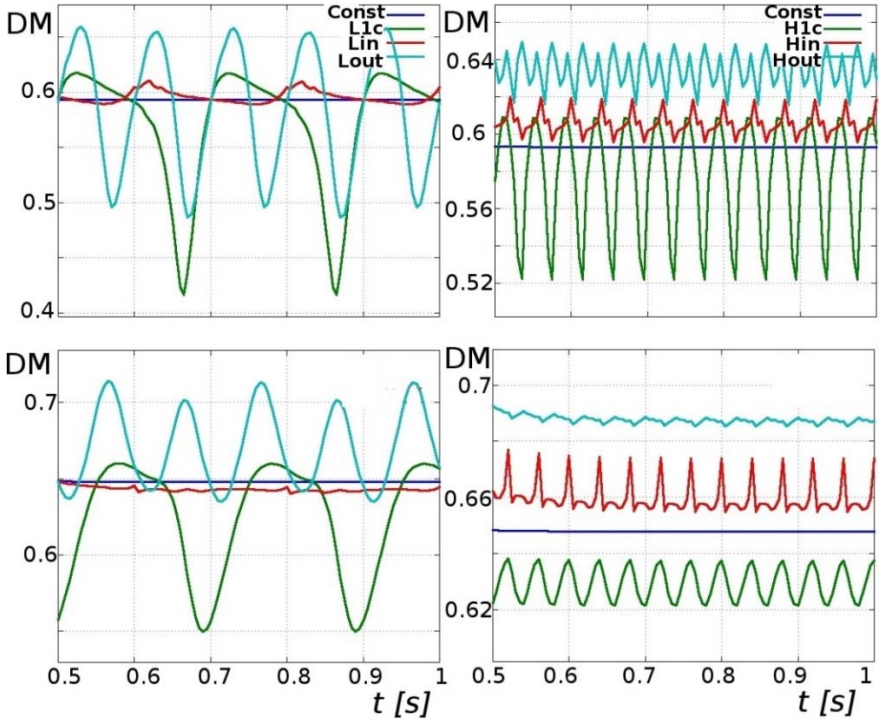

Fig. 6. Changes of DM in time in the B_C (upper row) and B_W (lower row) cross-sections. The left column shows low frequency results and the right column shows high frequency results. The horizontal axis shows time in seconds. High frequency and out-of-phase BC improve the mixing by 6-7% when compared with the reference case

4.2. Quality of mixing in the B location of the 2D type serpentine mixer

Some results are more optimistic at the end of the channel, in the **B** location. The upper row of Figure 7 shows the characteristics of the DM parameter in the middle of the channel (location B_C). Here, it can be seen that there is no improvement when compared with the reference case, for any combination of low frequency pulsation BC. The quality of the mixture even decreased due to its strong time dependency.

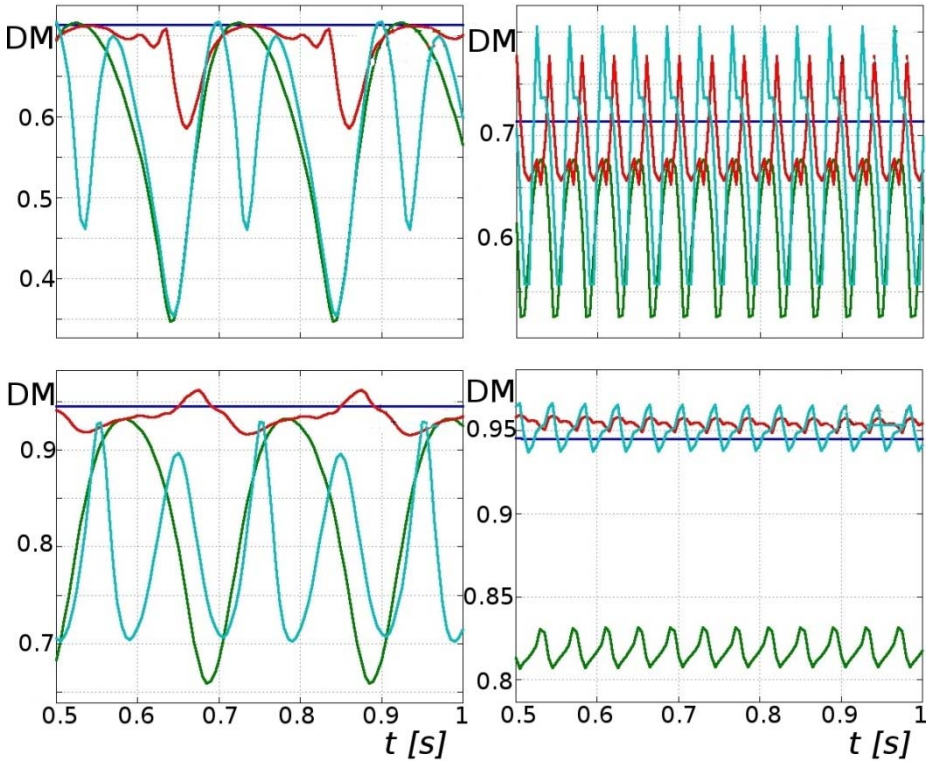

Fig. 7. Changes of *DM* in time in the A_C (upper row) and B_C (lower row) cross-sections for the 3D type serpentine mixer. The left column shows low frequency results and the right column shows high frequency results. The horizontal axis shows time in seconds. High frequency and out-of-phase BC improve the mixing only slightly when compared with the reference case

Table 3. *DM* averaged in time in the B_C and B_W cross-sections

BC type	DM at B_C	DM at B_W
1 – Const	0.593	0.648
2 – *L1c*	0.573	0.624
3 – L_{in}	0.595	0.643
4 – L_{out}	0.584	0.671
5 – *H1c*	0.577	0.671
6 – H_{in}	0.601	0.629
7 – H_{out}	0.634	0.688

The results are more optimistic for high frequency pulsation BC, as can be seen on the right column of Figure 6. The time averaged DM parameter shows that the out-of-phase (H_{out}) BC can produce 7% and 6% improvement for the location B_C and B_W respectively, Table 3. This phenomenon is caused by extension of the interface area. Through the action of the high frequency pulsations, the fluid elements are deformed and folded. Moreover, for this type of micromixer the size of the interface area increases

with the number of bends (Malecha et al., 2009; Yi and Bau, 2003). Therefore, the impact of the high frequency pulsation BC is better seen at a location further away from the T-junction. Moreover, just as importantly, the amplitude of the inlet pulsations is only slightly transferred onto the time characteristic of the mixture quality and almost completely suppressed in the B_W location.

4.3. Quality of mixing of the 3D type serpentine mixer

In this section, detailed measurements for the 3D type serpentine mixer are presented. Table 4 shows the time averaged values of the DM parameter for A_C and A_W cross-sections. First of all, it can be noticed that the 3D mixer performs by about 90% better than the 2D mixer at the corresponding locations and even by about 20% better than the 2D mixer at the **B** location. Similarly, like before, neither low nor high frequency pulsations are able to produce any better results than the simple constant velocity BC. The upper row of Fig. 7 shows the changing of the DM parameter in time at A_C location for low and high frequency pulsation BC. As in the case of the 2D mixer, the amplitude of the oscillations is still significant for almost all types of BCs at the location A_C.

Table 4. *DM* averaged in time in the A_C and A_W cross-sections

BC type	DM at A_C	DM at A_W
1 – Const	0.714	0.737
2 – *L1c*	0.606	0.681
3 – L_{in}	0.687	0.758
4 – L_{out}	0.581	0.625
5 – *H1c*	0.613	0.660
6 – H_{in}	0.689	0.765
7 – H_{out}	0.677	0.783

Table 5 shows the time averaged values of the DM parameter for B_C and B_w cross-sections. It can be noticed that the 3D mixer produces about 95% efficiency for the simple constant velocity BC. The bottom row of Fig. 7 shows time plots of the DM parameter for low and high pulsation BCs at the B_C location. The amplitude of the oscillations is still significant in the case of low frequency BC, but high frequency BC can suppress initial pulsations significantly and produce a very slight improvement in mixing by about 1%. This confirms that the best choice of BC is out-of-phase and high frequency pulsations, but the general conclusion is that any type of BCs cannot make the 3D type serpentine mixer more efficient.

Table 5. *DM* averaged in time in the B_C and B_W cross-sections

BC type	DM at B_C	DM at B_W
1 – Const	0.945	0.951
2 – *L1c*	0.831	0.819
3 – L_{in}	0.934	0.951
4 – L_{out}	0.790	0.803
5 – *H1c*	0.818	0.801
6 – H_{in}	0.954	0.962
7 – H_{out}	0.951	0.960

5. RESULTS, PART II

In this section, a faster and simplified method for the evaluation of mixing quality will be introduced. First, it will be compared with the results of the full 3D model from the previous section. Next, it will be used to evaluate the 2D type serpentine micromixer performance under various types of vibrations: rotational, vertical and horizontal, and different frequencies of oscillations. The results presented in the *Results, part II* section are obtained using the *interDyMFoam* solver implemented in OpenFOAM. It solves for 2 incompressible, isothermal immiscible fluids using a VOF (volume of fluid) phase-fraction based interface capturing approach, with optional mesh motion and mesh topology changes.

5.1. Simplified 2D model. Comparison with full 3D model

As previously mentioned, the performance of the micromixers can be enhanced by increasing the contact interface between mixing fluids. That is why it seems that it is sufficient to calculate only the size of the contact interface as a function of proposed (investigated) perturbing mechanism to evaluate its influence on mixing qualities. To achieve this goal, we propose the 2D calculations of two immiscible fluids, based on VOF method. Such an approach has three main advantages: 1) because evaluation is based only on distortion of the contact interface, the mass diffusion mechanism is excluded from the model (knowledge of the mass diffusion coefficient D is not necessary), 2) immiscibility assures the ease of the interface tracking and its detection, 3) two-dimensionality makes calculations much faster.

From the previous calculations, it may be concluded that the most efficient BCs for mixing were those with out-of-phase and high frequency (25 Hz) pulsations. We may then inquire as to whether a further increase of the pulsation frequency would improve the mixing quality, or what is the limit of frequency beyond which there is no improvement? Rather than performing the time-consuming 3D calculations, this can be evaluated using the proposed method based on 2D VOF model.

Figure 8 shows a comparison of the results based on the full 3D model and the 2D VOF model. The horizontal axis shows the frequency of the BC pulsations and the vertical axis shows the normalised quality of the mixing. In the case of the full 3D model, the quality of mixing was calculated using formula (9) and normalised by the value of DM for a constant BC case. In the case of the simplified 2D method, a normalised quality of mixing was calculated as time averaged length of the contact interface:

$$L = \frac{1}{L_c}\frac{1}{T_2 - T_1}\int_{T_1}^{T_2} s(t)dt \tag{10}$$

where $s(t) = \int_{C(t)} \sqrt{dx^2 + dy^2}$ is the length of the contact interface for time t, $T_1 = 0.25$ s, $T_2 = 1$ s and L_C is length of the interface for the constant BC case. Time average in Eq. (10) did not start from zero because at the initial condition the channel was filled only with one fluid. Time T_1 was chosen to be beyond the initial transient flow resulting from the initial condition.

In Equation (10), $L = 1$ means that the length of the interface, between mixing fluids, is the same as the length of the interface in the case of the reference flow. Hence, no improvement in mixing is expected. If $L > 1$, the length of the interface would be longer than that in the case of the reference flow. Hence, the mixing could potentially be improved, because there would be a greater contact area between the two fluids.

It can be seen from Fig. 8 that the full and simplified models suggest that the best micromixer performance can be achieved with a frequency range of 25-35 Hz, above which there is no further improvement. The full model has its peak at 25 Hz, whereas the simplified model has two peaks at 30

Hz and 35 Hz. The double peak structure suggests that 35 Hz might be close to resonant frequency of the considered system, for which a sudden increase of the interface distortion can be expected. What is worth mentioning here is the fact that calculations of the simplified model were 10 times faster than those of the full 3D model.

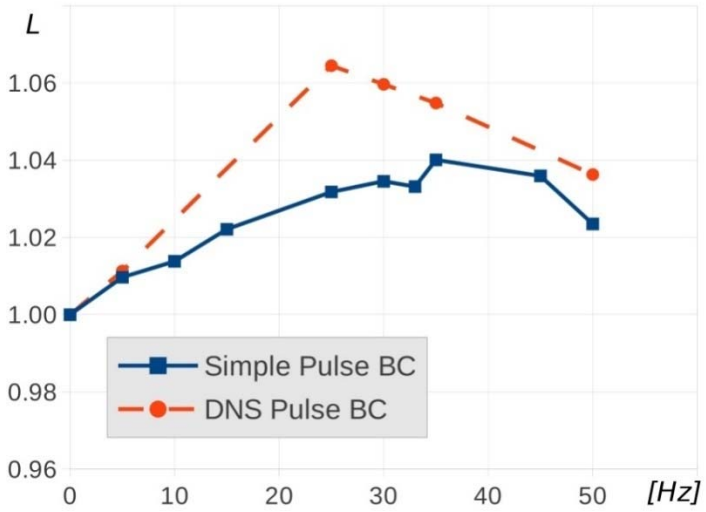

Fig. 8. Comparison of the mixing quality based on full 3D model (DNS) and 2D VOF model (Simple) normalised in respect to constant BC result

Figure 9 shows the shape of the contact interfaces for frequencies of 25, 35 and 50 Hz, at the time instances when they are the longest. It can be seen that the 35 Hz interface develops highly curved small structures, which can be observed in various places and times. This was not observed in lower and higher frequencies.

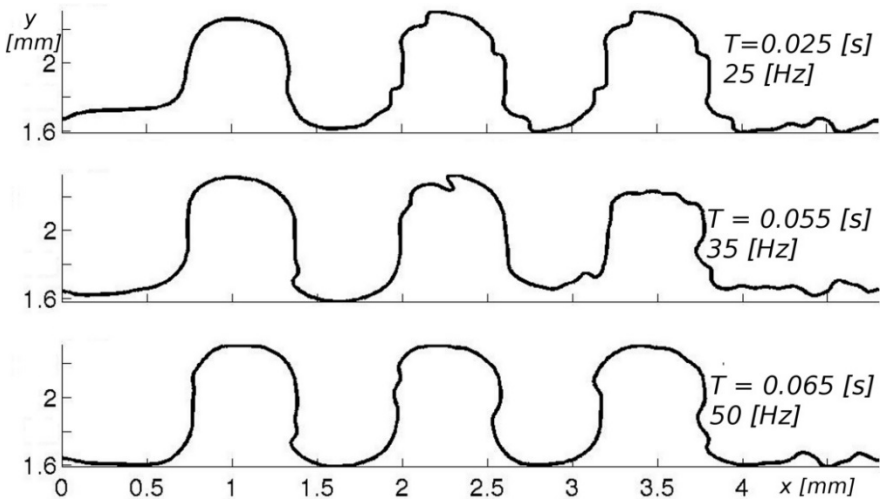

Fig. 9. Contact interface in its longest state for frequency of 25, 35 and 50 Hz

5.2. Various vibrations of the micromixer

Second possible means of the active improvement of the micromixers performance are vibrations of the whole microchip. Below are presented estimates of the mixing quality based on the proposed simplified method under various vibration movements and different frequency of vibration oscillations. Rotational, vertical and horizontal vibrations were investigated with the frequency up to 50 Hz. Figure 10 shows the micromixer under rotational vibrations in its maximum angles of inclination

(± 5 degrees) with a pivoting point located in the centre of the mass. Vertical and horizontal vibrations had amplitude of $\pm 2\times10^{-4}$ m from the neutral position.

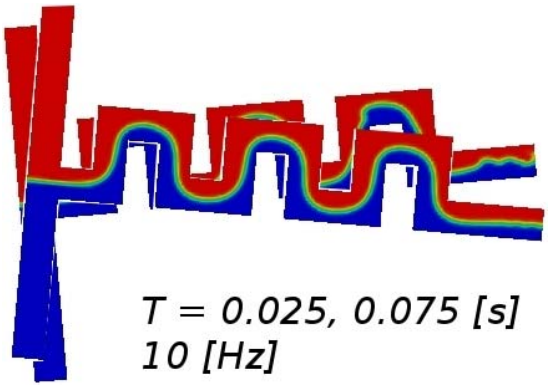

Fig. 10. Micromixer under rotational vibrations in its maximum angles of inclination (5 degrees)

Figure 11 shows the comparative results of mixing qualities under rotational, vertical and horizontal vibrations. Rotational and vertical vibrations show better mixing performance with higher oscillations. Surprisingly, horizontal vibrations do not show any improvement. The frequency of 30-35 Hz indicates a critical value above which a significantly faster change of the interface length is observed. Above this value, the interface was characterised with a very significant curvature and distortion to the limit of being broken, Figure 12.

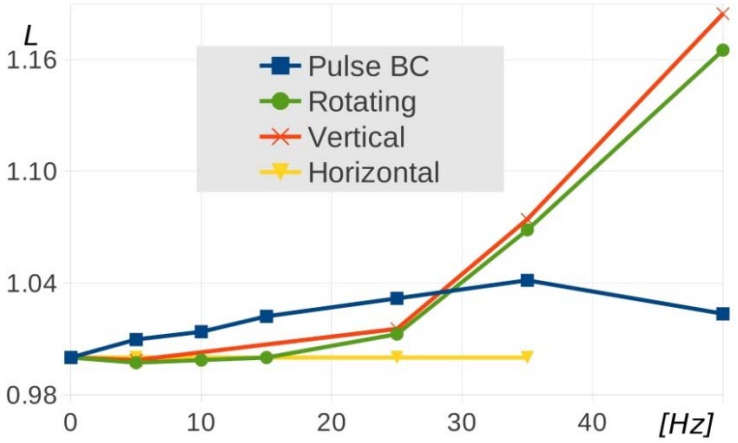

Fig. 11. Comparative results of mixing qualities under rotational, vertical and horizontal vibrations

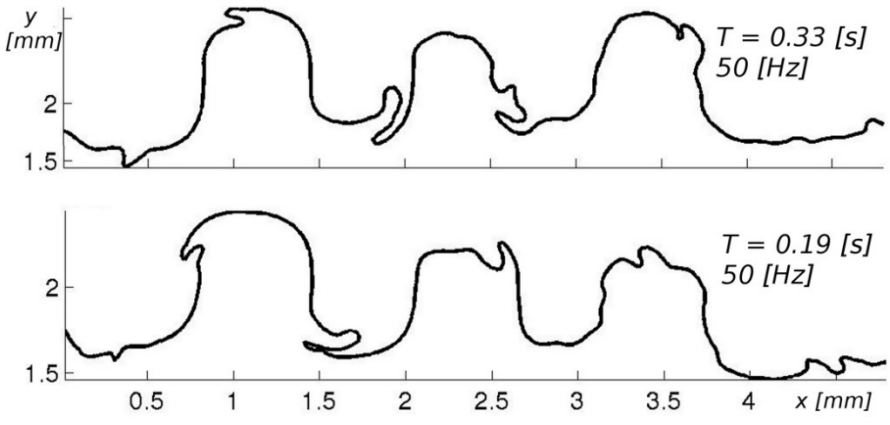

Fig. 12. Contact interface in its longest state for frequency 50 Hz for rotational (top) and vertical (bottom) vibrations

Horizontal vibrations do not cause any improvement in mixing qualities. Frequency of 30-35 Hz indicates a critical value above which a significantly faster change of the interface length can be seen.

6. CONCLUSIONS

The presented results have shown that mixing quality could be improved by ~ 6-7% in the 2D type serpentine micromixer, if out-of-phase high frequency (25 Hz) pulsations of the entering fluids were to be applied. This improvement was visible in both the centre of the channel and close to the wall. Moreover, results showed that the frequency of 25 Hz is optimal, above which mixing quality deteriorated.

The time averaged results of the low frequency (5 Hz) pulsations showed some improvement as well, but a positive interpretation for this could be very misleading. An important disadvantage of low frequency pulsations BC was in the transmission of the initial amplitude of perturbations directly onto mixture quality. Mixture quality was strongly time dependent and its instantaneous value was significantly below that of the reference case. This may suggest that a similarly unfavourable phenomenon may be present in the simple geometry micromixers as well even though time averaged improvement was observed by Neild et al. (2010). On the other hand, the presented results have shown the very important advantage of the high frequency pulsations BC. In this case, the initial BC perturbation amplitude was significantly reduced and the instantaneous mixing quality was always above that of the reference case.

The proposed simplified method compared well with the full 3D model. Operating at an order of magnitude faster than the 3D model, it can be used as a prognostic tool to evaluate the possible improvement of the mixing quality under various types of passive and active perturbations of the flow field. As an example, it was used to evaluate possible improvements with the implementation of rotational, vertical and horizontal vibrations of the microchip. Surprisingly, horizontal vibrations do not show any improvement regardless of the frequency of vibrations.

The numerical results for the 3D type serpentine micromixer proved its excellent mixing properties, which could still be slightly improved by ~ 1% if high frequency pulsations BC were used. The applied numerical model was not able to tell if the high curvature of the channels could potentially lead to the undesired phenomenon of microbubble formation. A numerical study of this problem can be an important extension to the presented work.

The efficiency of mixing obtained by flow pulsation in comparison with device vibration strongly depends on frequency. For low frequencies (up to 25 Hz) mixing is slightly better for flow pulsation approach. Device vibration is much more efficient at higher frequencies (above 30 Hz). However, vibration approach is more complex and challenging for realization and integration with a real microfluidic structure. Moreover, micromixers with a vibration system run a risk of damage during operation.

The authors would like to thank Chia-Luen Lee for her careful proofreading and language corrections of the above article. The authors wish to thank National Science Centre (DEC-2013/09/D/ST7/03953) and Wrocław University of Technology (B30104) for financial support. This research was supported in part by PL-Grid Infrastructure (http://www.plgrid.pl/en).

SYMBOLS

c	concentration
D	diffusion coefficient, m^2/s
DM	weighted standard deviation
F	force, N
H	height of the channel in y (vertical) direction, m
J	diffusion flux, $mol/(m^2 \cdot s)$
L	length of the contact interface
L_C	length of the interface for the constant boundary condition case, m
p	pressure, Pa
Re	Reynolds number
$s(t)$	length of the contact interface for time t, m
t	time, s
U	characteristic velocity, m/s
$\mathbf{u} = (u, v, w)$	fluid velocity in x, y, z direction, m/s
u_m	averaged u (horizontal) velocity along y (vertical) cross-section of the channel, m/s

Greek symbols

μ	dynamic viscosity, Pa·s
ρ	density, kg/m^3
σ	standard deviation

Subscripts

1, 2	number of fluid

REFERENCES

Bałdyga J., Bourne, J. R., 1984. Mixing and fast chemical reaction-VIII: Initial deformation of material elements in isotropic, homogeneous turbulence. *Chem. Eng. Sci.*, 39, 329-334. DOI: 10.1016/0009-2509(84)80031-7.

Batchelor G.K., 2000, *An Introduction to Fluid Dynamics*. Cambridge University Press, Cambridge (UK).

Dziuban J.A., Mróz J., Szczygielska M., Małachowski M., Górecka-Drzazga A., Walczak R., Buła W., Zalewski D., Nieradko L., Łysko J., Kosztur J., Kowalski P., 2004. Portable gas chromatograph with integrated components. *Sens. Actuators A*, 115, 318-330. DOI: 10.1016/j.sna.2004.04.028.

Glasgow I., Aubry N., 2003. Enhancement of microfluidic mixing using time pulsing. *Lab Chip*, 3, 114-120. DOI: 10.1039/B302569A.

Gravesen P., Branebjerg J., Jensen O.S., 1993. Microfluidics – A review. *J. Micromech. Microeng.*, 3, 168-182. DOI: 10.1088/0960-1317/3/4/002.

Groß G., Thelemann T., Schneider S., Boskovic D., Kohler J., 2008. Fabrication and fluidic characterization of static micromixer made of low temperature cofired ceramic (LTCC). *Chem. Eng. Sci.*, 63, 2773-2784. DOI:10.1016/j.ces.2008.02.030.

Hessel V., Lowe H., Schonfeld F., 2005. Micromixer a review on passive and active mixing principles. *Chem. Eng. Sci.*, 60, 2479-2501. DOI: 10.1016/j.ces.2004.11.033.

Kudela H., Malecha Z.M., 2009. Eruption of a boundary layer induced by a 2D vortex patch. *Fluid Dyn. Res.*, 41, 055502. DOI: 10.1088/0169-5983/41/5/055502.

Liu P., Li X., Greenspoon S.A., Scherer J.R., Mathies R.A., 2011. Integrated DNA purification, PCR, sample cleanup, and capillary electrophoresis microchip for forensic human identification. *Lab Chip*, 11, 1041-1048. DOI: 10.1039/c0lc00533a.

Malecha K., 2013. A PDMS-LTCC bonding using atmospheric pressure plasma for microsystem applications. *Sens. Actuators B*, 181, 486-493. DOI: 10.1016/j.snb.2013.01.094.

Malecha K., Golonka L.J., Bałdyga J., Jasińska M., Sobieszuk P., 2009. Serpentine microfluidic mixer made in LTCC. *Sens. Actuators B*, 143, 400-413. DOI: 10.1016/j.snb.2009.08.010.

Malecha K., Pijanowska D.G., Golonka L.J., Kurek P., 2011. Low temperature co-fired ceramic (LTCC)-based biosensor for continuous glucose monitoring. *Sens. Actuators B*, 155, 923-929. DOI: 10.1016/j.snb.2011.01.002.

Malecha Z.M., Chorowski M., Polinski J., 2013. Numerical study of emergency cold helium relief into tunnel using a simplified 3D model. *Cryogenics*, 57, 181-188. DOI: 10.1016/j.cryogenics.2013.07.006.

Malecha Z.M., Mirosław L., Tomczak T., Koza Z., Matyka M., Tarnawski W., Szczerba D., 2011. GPU-based simulation of 3D blood flow in abdominal aorta using openfoam. *Archives of Mechanics*, 63, 137-161.

Manz A., Graber N., Widmer M., 1990. Miniaturized total chemical analysis systems: A novel concept for chemical sensing. *Sens. Actuators B*, 1, 244-248. DOI: 10.1016/0925-4005(90)80209-I.

Monnery W.D., Svrcek W.Y., Mehrotra A.K., 1995. Viscosity: A critical review of practical predictive and correlative methods. *Can. J. Chem. Eng.*, 73, 3-40. DOI: 10.1002/cjce.5450730103.

Neild A., Wah Ng T., Sheard G.J., Powers M., Oberti S., 2010. Swirl mixing at microfluidic junctions due to low frequency side channel fluidic perturbations. *Sens. Actuators B*, 150, 811-818. DOI: 10.1016/j.snb.2010.08.027.

Nguyen N.-T., 2012. *Micromixers: Fundamentals, design and fabrication*. 2nd edition, Elsevier, Oxford (UK).

Nguyen N.-T., Wu Z., 2005. Micromixers - A review. *J. Micromech. Microeng.*, 15, R1-R16. DOI: 10.1088/0960-1317/15/2/R01.

Oberti S., Neild A., Wah Ng T., 2009. Microfluidic mixing under low frequency vibration. *Lab Chip*, 9, 1435-1438. DOI: 10.1039/b819739c.

OpenFOAM, 2009. *The Open Source CFD Toolbox User Guide*.

Ottino J.M., Wiggins S., 2004. Introduction: Mixing in microfluidics. *Phil. Trans. R. Soc. Lond. A*, 362, 923-935. DOI: 10.1098/rsta.2003.1355.

Wiggins S., Ottino J.M., 2004. Foundations of chaotic mixing. *Phil. Trans. R. Soc. Lond. A*, 362, 937-970. DOI: 10.1098/rsta.2003.1356.

Yi M., Bau H.H., 2003. The kinematics of bend-induced mixing in microconduits. *Int. J. Heat Fluid Flow*, 24, 645-656. DOI: 10.1016/S0142-727X(03)00026-2.

Received 01 January 2014
Received in revised form 24 April 2014
Accepted 20 July 2014